Durability Analysis of CFRP Adhesive Joints: A Study Based on Entropy Damage Modelling Using FEM

Yutong Li , Huachao Deng , Maruri Takamura , Jun Koyanagi *

Posted Date: 27 September 2023

doi: 10.20944/preprints202309.1805.v1

Keywords: numerical simulation; composite laminates; entropy-based strength degradation; CFRP transverse cracking behavior; fatigue

Article

Durability Analysis of CFRP Adhesive Joints: A Study Based on Entropy Damage Modelling Using FEM

Yutong Li, Huachao Deng, Maruri Takamura and Jun Koyanagi *

Department of Materials Science and Technology, Tokyo University of Science, Japan
* Corresponding author: koyanagi@rs.tus.ac.jp

Abstract: Experimental methodologies for fatigue lifetime prediction are time-intensive and susceptible to environmental variables. While the cohesive zone model is popular for predicting adhesive fatigue lifetime, entropy-based methods have also shown promise. This study aims to provide an understanding of the durability characteristics of CFRP adhesive joints by incorporating an entropy damage model within the context of the finite element method (FEM), examined the effects of different adhesive layer thicknesses on SLS models. As the adhesive layer increased in thickness, DAMAGE VARIABLES initially rose and then declined, peaking at 0.3mm. This finding provides crucial understanding into the stress behavior at the resin-CFRP interface and the resin's fatigue mechanisms.

Keywords: numerical simulation; composite laminates; entropy-based strength degradation; CFRP transverse cracking behavior; fatigue

1. Introduction

The adhesive bonding technology has been developed widely to join similar and dissimilar materials (glass, metals, plastics and ceramics) due to its many advantages versus the other methods of joining, e.g., fastening, riveting, brazing and welding [1–3]. There has been an increasing use of adhesive bonding technology in aerospace industry [4–8] due to its superiority over conventional joining technologies in many aspects such as high specific strength, flexibility, damage tolerance and fatigue resistance. In the bonded structures, the adhesive layer is usually sprayed between two or more adherends [9]. Differing from the adherends, the strength of adhesive layer is much weaker, and under the cyclical mechanical or thermal loadings the delamination usually occurs in it [10–12]. As the delamination progresses, the bond strength decreases drastically and the durability of bonded joints will be affected seriously. Thus, the accurate fatigue lifetime estimations of adhesive layer under cyclical loading are of critical significance.

In the early works, the experiment methodologies were extensively utilized to investigate the strength and fatigue lifetime of adhesive-bonding structures. Ishii *et. al.* [13] carried out a series of fatigue tests on three kinds of adhesively bonded joint specimens: butt joint, scarf joint and thick adherend lap-shear joint to investigate the fatigue failure criterion for the CFRP/metal joints under multiaxial stress condition. Based on two stress singularity parameters, Ishii *et. al.* [14] also proposed the evaluation method for the endurance limit for adhesively bonded single, single-cracked and single step double-lap joints. Ferreira *et. al.* [15] studied the effects of layer orientation, lap joint length and water immersion on the fatigue performance of adhesive used with polypropylene based composites. The results revealed that the effect of water exposure on the fatigue behavior was mainly conditioned by the water temperature and to a lesser degree by the exposure time. Zhang *et. al.* [16] investigated environmental effect on fatigue behavior of adhesively-bonded pultruded joints subjected to a constant amplitude load. It was found that environment has a considerable effect on the fatigue behavior of the examined joints. Increased temperature seems to shorten specimen fatigue life. This phenomenon is more pronounced in the presence of high humidity levels. Tang *et. al.* [17]

 doi:10.20944/preprints202309.1805.v1

pointed out that both static and fatigue strength values decrease with increase of bond line thickness, and demonstrated how the generalized stress intensity factors can be applied for fatigue failure prediction. Recently, Reis *et. al*. [18] conducted the investigations into the effect of load frequency on the fatigue behavior of adhesively-bonded steel lap joints, and the results indicated that load frequency was a key factor to affect fatigue lifetime of adhesive: for higher shear stress amplitudes, the frequency presented only a marginal effect on fatigue life. On the other hand, for lower shear stress amplitudes, the fatigue life of the adhesive joints was greatly dependent on the frequency level. Schneider *et. al*. [19] used stress-life method to estimate the fatigue lifetime of joints bonded with a toughened epoxy adhesive at different temperatures, and experimental results showed that increasing temperature will reduce lifetime.

Considering that the experimental methodologies are often time-consuming, and results can be affected by the environmental conditions, such as the size of the specimen and loading condition, researchers have been seeking for efficient numerical methods for predicting fatigue lifetime accurately. Among the numerical methods for predicting the fatigue lifetime of adhesive, the cohesive zone model (CZM) based on the damage mechanics is most widely used. Khoramishad *et. al*. [20] developed a bi-linear traction-separation description in a CZM to simulate the progressive damage in the adhesively bonded joints. Jimenez and Duddu [21] investigated the sensitivity of CZM for high-cycle fatigue delamination, and these sensitivity investigations showed that the separation and strain-based fatigue damage functions were highly sensitive to cohesive stiffness and strength parameters. Fekih *et. al*. [22] devised novel adhesive test assemblies consisting of a rigid ceramic component bonded to a resonant flexible epoxy-fiber glass (E-glass) support, and derived an intrinsic fatigue damage law of adhesive. In addition to the well-known stress-based or energy-based methods for the estimation of fatigue life [23–26], approaches based on irreversible thermodynamics [27–29] were also proposed to investigate the failure mechanism and long-term lifetime of solid materials. It's widely recognized that both irreversible microplastic deformation and internal friction can lead to permanent degradation, as seen in plastics. In the view of thermodynamics, these irreversible degradations can be measured by entropy, which is a non-negative quantity and can serve as a basis for the damage evolution metric for elastic and inelastic deformations. When the entropy generation of a material reaches a threshold value called fracture fatigue entropy (FFE) [30,31], final failure occurs. Many publications have been reported to show that the estimation of fatigue life based on entropy is promising. It should be noted that the fracture fatigue entropy of material is also constant, even in the case where A656-grade steel is subjected to ultrasonic vibration at 20 kHz [32].

While the entropy-based failure criterion is commonly used to predict the fatigue life of metal components, its use for assessing the prolonged life of CFRP under cyclic loading is less established. Huang et al. [33] examined the influence of stacking sequences on CFRP ply's internal friction and fracture fatigue entropy. Additionally, the fatigue life estimation of CFRP was assessed, considering both confidence levels and reliability. Koyanagi et al. [34–38] recently formulated a computational approach integrating entropy damage to analyze the failure mechanism of a viscoelastic matrix and CFRP cross-ply laminates.

This study aims to provide an understanding of the durability characteristics of Carbon Fiber Reinforced Polymer (CFRP) adhesive joints by incorporating an entropy damage model within the context of the finite element method (FEM). Through FEM analyses under cyclic loading, it was observed that energy dissipates due to viscosity with repeated loads, causing an increase in entropy and resulting in damage. Alterations in stress distribution were observed in relation to this process. Traditional S-N curve analyses seem inadequate for these observed changes. Analyses were conducted with varied adhesive layer thicknesses, indicating a potential optimal value for thickness.

Preprints (www.preprints.org) | NOT PEER-REVIEWED | Posted: 27 September 2023 doi:10.20944/preprints202309.1805.v1

Nomenclatures

$\boldsymbol{\varepsilon}$, $\Delta\boldsymbol{\varepsilon}$: Total strain tensor, increment of total strain tensor
$\boldsymbol{\varepsilon}^{ve}$, $\boldsymbol{\varepsilon}^{vp}$: Viscoelasticity strain tensor, viscoplasticity strain tensor
$\boldsymbol{\sigma}$, $\Delta\boldsymbol{\sigma}$, $\mathbf{s}$: Stress tensor, increment of stress tensor, deviatoric stress tensor
p, $\mathbf{I}$: Hydrostatic stress, second order identity tensor
D, D_{cr}: Damage variable, critical damage variable
s, s^f: Entropy generation, final fracture entropy
g: Nonlinear coefficient
t, t': Time
W: Dissipated energy
α_d: Damage parameters
$\mathbf{E}^r$: Relaxation tensor
$\mathbf{H}$: Viscosity matrix
$\mathbf{M}$: Constant matrix
$\mathbf{D}$, E_0, ν: Stiffness matrix, initial Young's modulus, Poisson's ratio
E_n η_n: Viscoelasticity properties of Maxwell elements
σ_{eqv}, ε_{eqv}^{vp}: Equivalent stress, equivalent viscoplastic strain
η^{vp}, η_0, α, β, χ: Viscoplasticity coefficients
$\boldsymbol{A}$, $\boldsymbol{V}$: Generalized thermodynamic force and internal flow vectors
T, $\boldsymbol{Q}$: Temperature, heat flux vector

2. Numerical methodology

2.1. Entropy-based failure criterion

In this study, the viscosity of matrix resin is addressed by the viscoelastic model using 15 Maxwell elements as shown in **Fig**ure 1, in which the total strain $\boldsymbol{\varepsilon}$ is decomposed into viscoelastic strain $\boldsymbol{\varepsilon}^{ve}$ and viscoplastic one $\boldsymbol{\varepsilon}^{vp}$ [13].

$$\boldsymbol{\varepsilon} = \boldsymbol{\varepsilon}^{ve} + \boldsymbol{\varepsilon}^{vp} \tag{1}$$

$$\boldsymbol{\varepsilon}^{vp} = \int_0^t \mathbf{H}^{-1}\boldsymbol{\sigma}\,\mathrm{d}t \tag{2}$$

where $\boldsymbol{\sigma}$ is the Cauthy stress tensor, t is time, and viscosity matrix $\mathbf{H}$ is

$$\mathbf{H} = \frac{\eta^{vp}}{(1+\nu)(1-2\nu)}\mathbf{M} \tag{3}$$

Preprints (www.preprints.org) | NOT PEER-REVIEWED | Posted: 27 September 2023 doi:10.20944/preprints202309.1805.v1

$$\mathbf{M}=\begin{bmatrix} 1-\nu & \nu & \nu & 0 & 0 & 0 \\ & 1-\nu & \nu & 0 & 0 & 0 \\ & & 1-\nu & 0 & 0 & 0 \\ & & & \frac{1}{2}-\nu & 0 & 0 \\ & Symmetry & & & \frac{1}{2}-\nu & 0 \\ & & & & & \frac{1}{2}-\nu \end{bmatrix} \tag{4}$$

$$\eta^{vp}=\eta_0\times\frac{1+e^{\beta\left(\varepsilon_{eqv}^{vp}/\sigma_{eqv}\right)^{\chi}}}{1+e^{\alpha(\sigma_{eqv}-\sigma_{vp0})}} \tag{5}$$

In Eq. (3)-(5), the related definitions of material properties are adopted from the reference.[38]

One viscoelastic constitutive relationship considering the damage variable D is expressed as [39]:

$$\boldsymbol{\sigma}(t)=(1-D)\int_0^t \mathbf{E}^r(t-t')\,g\dot{\boldsymbol{\varepsilon}}^{ve}\mathrm{d}t' \tag{6}$$

where the relaxation modulus $\mathbf{E}^r$ and nonlinear coefficient g are

$$\mathbf{E}^r(t)=\sum_{n=1}^{15}E_{ijkl}^n\,e^{-tE^n/\eta^n} \tag{7}$$

$$g=\frac{1}{1+\alpha\left(\frac{\sigma_{eqv}}{\sigma_0}\right)^m} \tag{8}$$

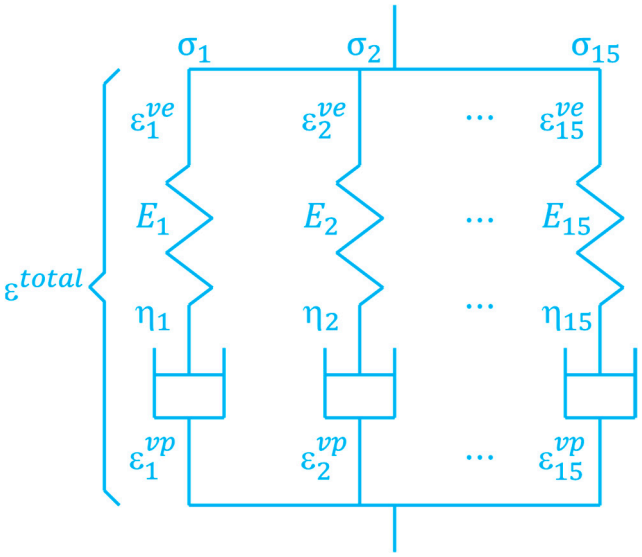

Figure 1. Viscoelastic model using 15 Maxwell's elements.

In this study, the entropy generation s is utilized to reveal the degradation of matrix resin and calculated as

$$s=\int_0^t\frac{1}{T}\boldsymbol{\sigma}:\dot{\boldsymbol{\varepsilon}}^{vp}\mathrm{d}t \tag{9}$$

where T is temperature, $\dot{\boldsymbol{\varepsilon}}^{vp}$ is visco-plastic rate. It is worth noting that the final fracture entropy s^f per unit volume of materials until fracture can be calculated by Eq. (9). Finally, the damage variable D related to the entropy generation is defined to address the degradation of properties:

$$D=\alpha_d\times\frac{s}{s^f}D_{cr} \tag{10}$$

where D_{cr} is user-defined critical damage value. Since the original UMAT is designed for standard fatigue tests, which usually requires many cycles to reach failure. To achieve fatigue failure with a

Preprints (www.preprints.org) | NOT PEER-REVIEWED | Posted: 27 September 2023 doi:10.20944/preprints202309.1805.v1

limited number of tension cycles, this study introduces a parameter, α_d, into the resin's characteristics, which serves to significantly amplify the damage incurred with each tension, thereby accelerating the completion of the simulation.

The developed entropy-based failure criterion has been implemented into a user-defined subroutine of Abaqus. The elongation of the dashpot, dissipated energy increment, and other parameters are computed to obtain the increment of entropy and damage, and update the stress components. Detailed explanation can be found in the reference [38].

2.2. Finite element modeling

This study uses the Abaqus CAE 2020 to create a Single Lap Shear (SLS) model (**Figure 2**). Two slabs of CFRP material, each with a length of 100mm, a thickness of 2mm, and a depth of 0.1mm, were bonded in the middle using a resin with a length of 20mm, a depth of 0.1mm, and a thickness ranging from 0.1 to 0.8mm (with a fixed increment 0.1mm). Resin and CFRP are constrained by tie type. SLS model is pinned at the left end, while a cyclic sinusoidal load, varying from 0 to 35MPa at load frequency 2Hz, is applied from the right end. To ensure numerical stability, displacement in the Z-direction is restrained.

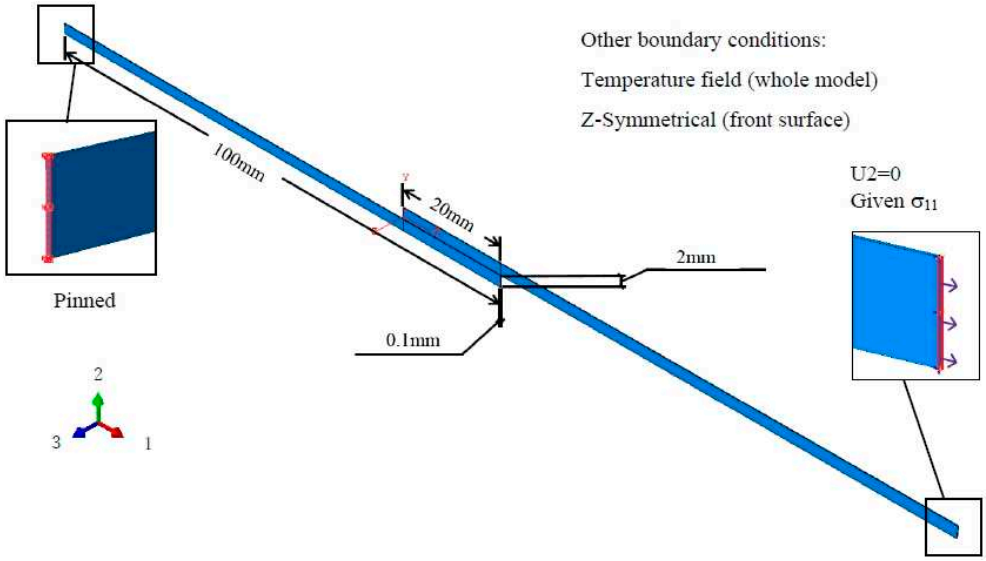

Figure 2. Dimension of SLS model.

As for the properties of the resin, it adopts a nonlinear viscoelastic viscoplastic material from the study of Kagawa et al. [40], which is implemented into Abaqus by the user subroutine UMAT. The CFRP is assumed as orthotropic elasticity because this study focuses on the failure of resin under cyclic loading. These properties are defined by engineering Constants listed in **Table 1**. As for the resin, detailed properties are presented in **Table 2**, which are adopted from the reference [38]. The resin portion is discretized by C3D8 elements with size of 0.1mm×0.1mm×0.1mm. In the case of a thickness of 0.1mm, the resin divides into a single layer of 1×200 elements. For the 0.2mm model, the total number of elements in the resin is 2×200, and so forth. Given the rotational symmetry of stress conditions on the resin's interfaces during tension, only the 200 elements on the upper interface of resin are considered in the following numerical analysis (**Figure 3**).

Table 1. Property parameters of CFRP.

E_1	E_2	E_3	Nu_{12}	Nu_{13}	Nu_{23}	G_{12}	G_{13}	G_{23}
15000	15000	294000	0.3	0.02	0.02	6000	18000	18000

Preprints (www.preprints.org) | NOT PEER-REVIEWED | Posted: 27 September 2023 doi:10.20944/preprints202309.1805.v1

Table 2. Property parameters of resin.

n	$E_n(\mathrm{MPa})$	$\eta_n(\mathrm{MPa{\cdot}s})$	Elasticity	
1	284	4.5×10^{2}	$E_0(\mathrm{MPa})$	4260
2	284	3.3×10^{3}	ν	0.3
3	284	1.2×10^{5}	Nonlinearity	
4	284	1.9×10^{6}	$\sigma_0(\mathrm{MPa})$	70
5	284	1.8×10^{7}	α	2
6	284	1.4×10^{8}	m	7
7	284	8.5×10^{8}	Viscoplastic strain	
8	284	5.0×10^{9}	$\eta_0(\mathrm{MPa{\cdot}s})$	1.0×10^{23}
9	284	3.0×10^{10}	$\sigma_{vp\_0}(\mathrm{MPa})$	0
10	284	1.9×10^{11}	α_{vp}	0
11	284	1.4×10^{16}	β_{vp}	0
12	284	1.3×10^{19}	χ	0
13	284	2.1×10^{22}		
14	284	1.3×10^{26}	Damage variables	
15	284	2.5×10^{29}	α_d	4

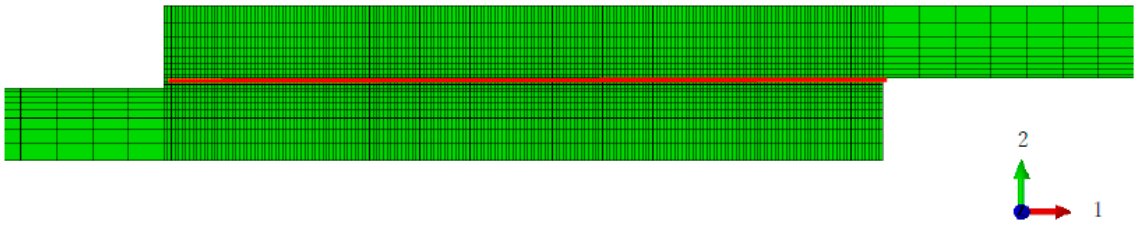

Figure 3. Mesh verifying of resin and the collection path of stress distribution.

Analysis procedure type is Static, General. Additionally, since failure typically initiates from the outermost elements, in this study, only the failure behavior of the first element on the top right of the resin is discussed (**Figure 4**).

Preprints (www.preprints.org) | NOT PEER-REVIEWED | Posted: 27 September 2023 doi:10.20944/preprints202309.1805.v1

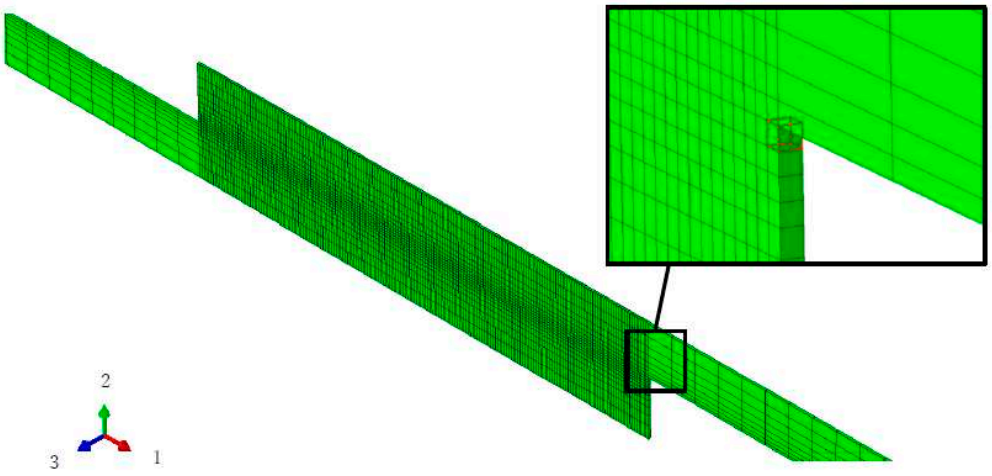

Figure 4. Elements enlarged view.

3. Results and discussions

3.1. Evolution of stress along the interface versus cyclic loadings

Taking the model with a thickness of 0.3mm as an example, stress distribution at the adhesive interface (upper surface) between the resin and CFRP is depicted in **Figure 5.** Throughout the tensile testing, the entire interface between the resin and the CFRP exhibits stress distribution. For clarity in the subsequent analysis, we designate the leftmost point of the resin as 0mm and the rightmost extent as 20mm. Regardless of whether it is s_{11}, t_{12} or s_{22}, stress peaks are evident at both ends of the resin during tension, with the peak at the right end surpassing that at the left. It is observed that the element located at 20mm (the furthest right) consistently failed first. As the stress peaks moving towards the center, the second element from the right began to fail. On the contrary, the position of the peak stress at the left end remained almost unchanged, and there were no cases of element failure on the left. At the onset of the first tension cycle, all elements on the resin's upper surface exhibit stress in the s_{11} and τ_{12} directions. Distinctively, the s_{22} stress behaves differently: it initially registers as zero in the central portion of the resin but displays pronounced peaks at both ends. As the tension cycles progress, these s_{22} stress peaks migrate towards the center, causing elements that initially displayed zero values to subsequently exhibit nonzero values.

When examining the centroidal stress of the uppermost right element of the resin, it can be observed that the stress values in s_{11}, τ_{12} and s_{22} are not constant but diminish with an increasing number of tension cycles. Furthermore, among these values, there is a consistent descending order in magnitudes from s_{22}, s_{11}, to τ_{12} as depicted in **Figure 6.** The magnitude of s_{11} remains at around half of s_{22}, and τ_{12} is initially close to that of s_{11}, but as the tension cycles increase, it diminishes to less than half of s_{11}. This simulation indicates that, even with a constant external load, the stress experienced by resin elements during fatigue test is not constant. This leads to the traditional S-N curve being inadequate in capturing such fatigue mechanisms. When studying material fatigue failure, factors beyond stress should be taken into consideration.

Preprints (www.preprints.org) | NOT PEER-REVIEWED | Posted: 27 September 2023 doi:10.20944/preprints202309.1805.v1

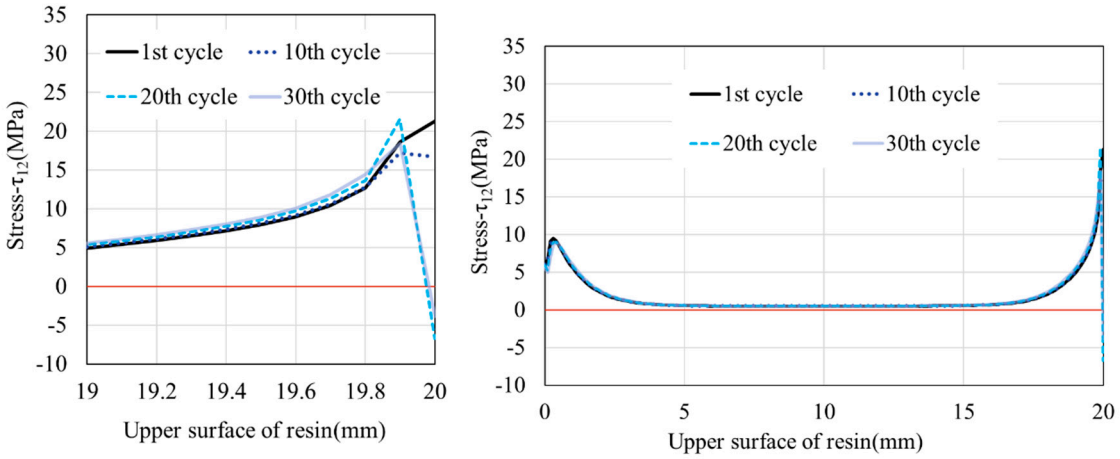

(a) s_{11} distribution and enlarged view at the right end

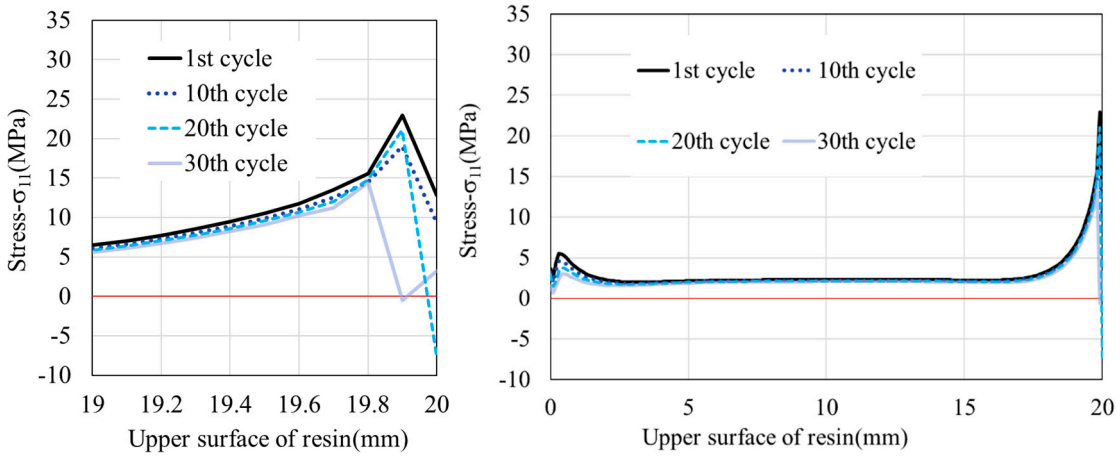

(b) τ_{12} distribution and enlarged view at the right end

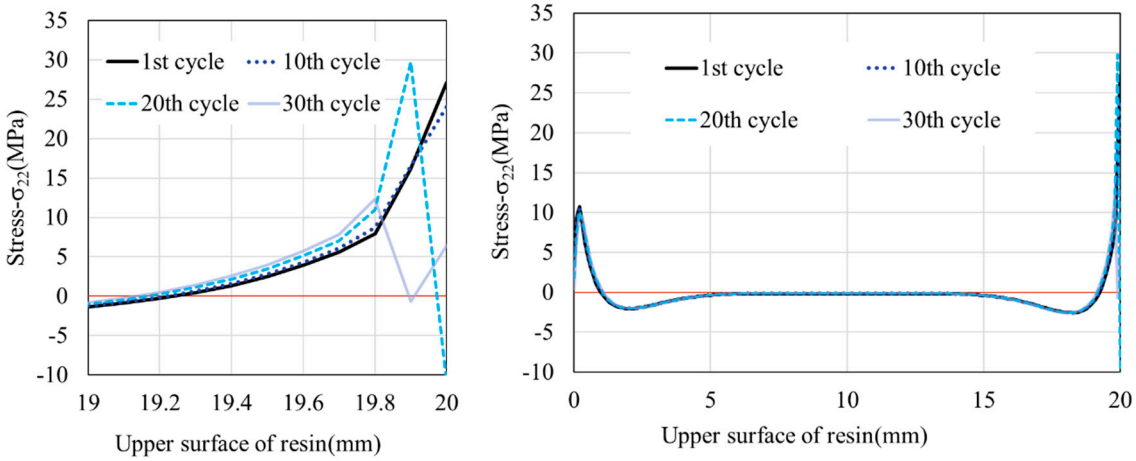

(c) s_{22} distribution and enlarged view at the right end

Figure 5. The stress distribution at different tension cycles for thickness of 0.3mm, data extraction locations refer to the red line in Figure 3.

Preprints (www.preprints.org) | NOT PEER-REVIEWED | Posted: 27 September 2023 doi:10.20944/preprints202309.1805.v1

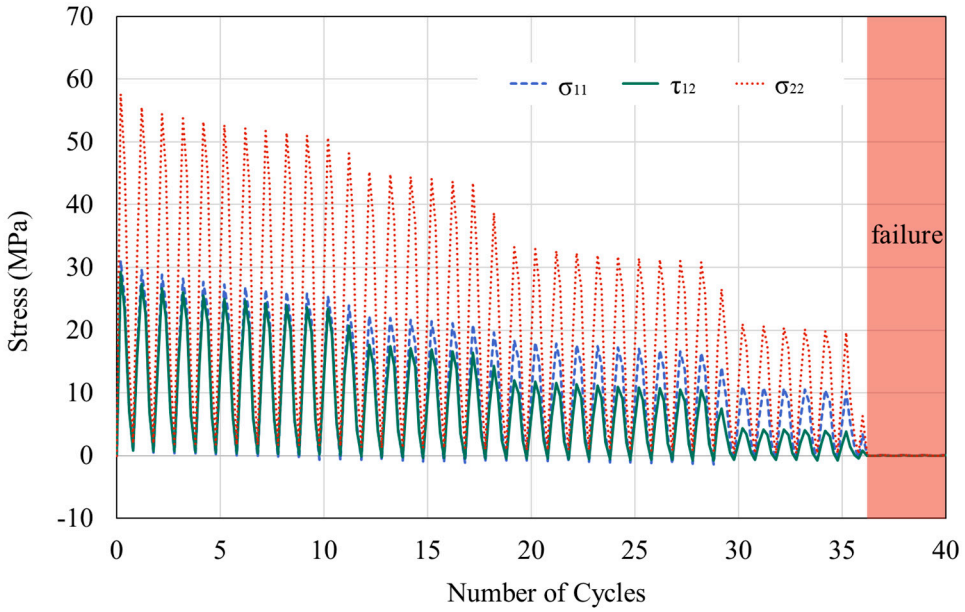

Figure 6. Variation of stress magnitude with the number of tension cycles, data extraction locations refer to the element highlighted by the red box in Figure 4.

3.2. Effect of adhesive thickness on the evolution of stress along the interface

In **Figure 7** and **Figure 8**, the stress distribution on the resin of different thicknesses is illustrated when the load reaches its peak for the first and the 20th times (To keep the figures clear and avoid too many overlapping lines, only some representative data points are shown). Although all models begin to fail from the rightmost end, for models thinner than 0.3mm, the stresses σ_{11}, τ_{12}, and σ_{22} at the left end exceed those at the right end, but for models 0.3mm and thicker, the stresses at the right end surpass those at the left. While the peak stress at the resin's right end oscillates with increasing tensile cycles. When comparing different resin thicknesses, thicker resins tend to exhibit higher stress peaks, as shown in **Figure 9**.

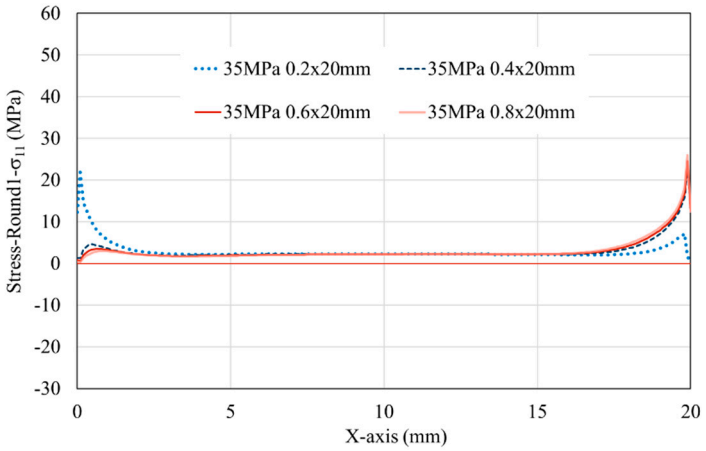

(**a**) S11

Preprints (www.preprints.org) | NOT PEER-REVIEWED | Posted: 27 September 2023 doi:10.20944/preprints202309.1805.v1

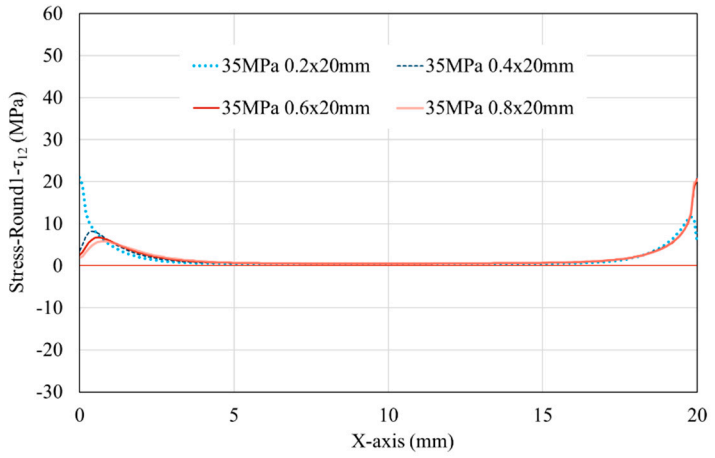

(**b**) τ12

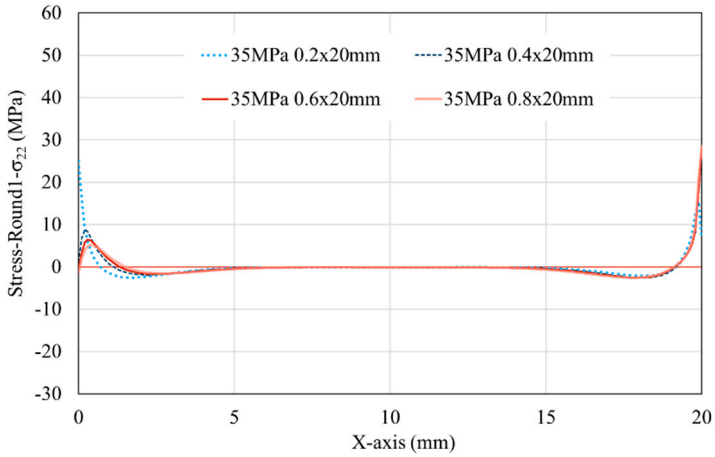

(**c**) S22

Figure 7. Stress distribution on the surface of resin with different thicknesses after the first tension, data extraction locations refer to the red line in Figure 3.

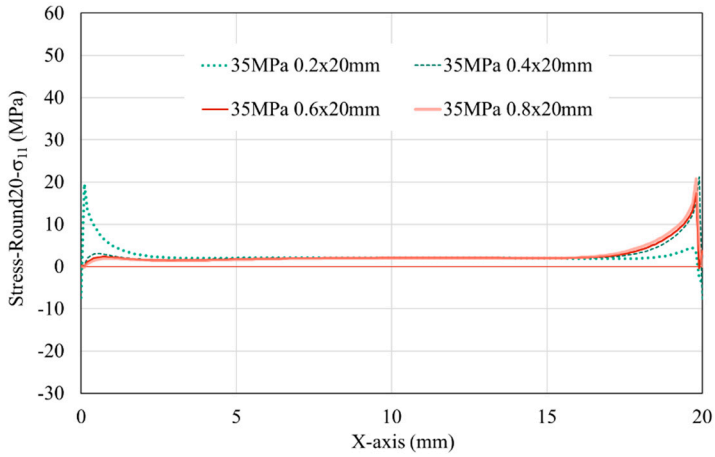

(**a**) S11

Preprints (www.preprints.org) | NOT PEER-REVIEWED | Posted: 27 September 2023 doi:10.20944/preprints202309.1805.v1

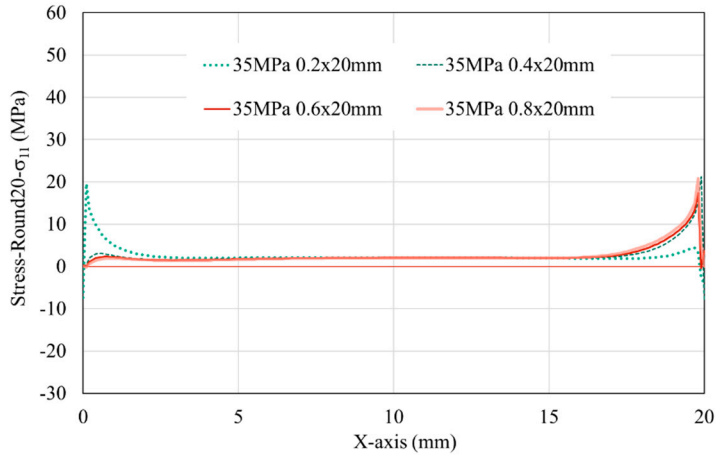

(**b**) τ_{12}

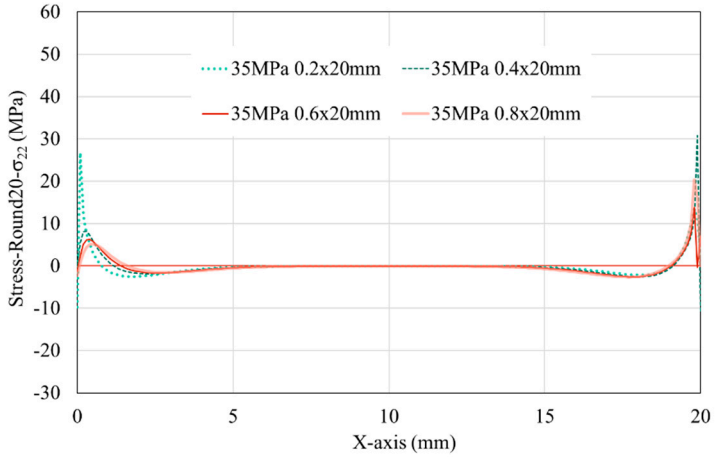

(**c**) S_{22}

Figure 8. Stress distribution on the surface of resin with different thicknesses after the 20th tension cycle, data extraction locations refer to the red line in Figure 3.

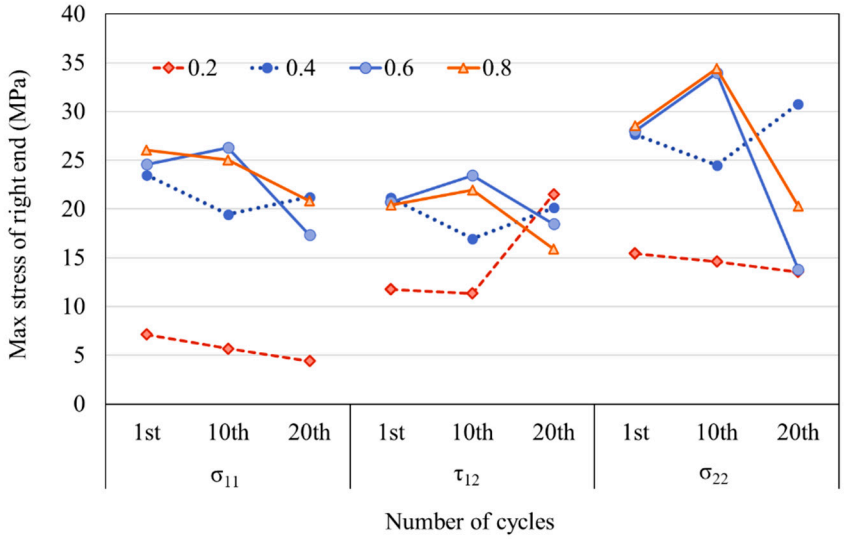

Figure 9. Relationship between the peak stress on the right side of the resin and thickness.

Preprints (www.preprints.org) | NOT PEER-REVIEWED | Posted: 27 September 2023 doi:10.20944/preprints202309.1805.v1

3.3. Relationship between number of cycles to failure (N_f) and thickness

Comparing the damage variables of the outermost element at the top right of the resin reveals that as thickness increases, the number of tensile cycles needed for the damage variables to reach the failure threshold of 0.25 (N_f) first rises and then falls, reaching a maximum at 0.3mm (**Figure 10**). As evident from the graph, the damage accumulation from the first tension occupies a significant portion, increase in damage variables after the first tension can be indicative of the failure tendencies of models with varying thicknesses. As the resin thickness increases, N_f initially rises and subsequently declines, reaching its peak at 0.3mm. Conversely, the increment in damage variables after the first tension exhibits an inverse pattern: for resin thicknesses below 0.3mm, it diminishes with increasing thickness; whereas for thicknesses beyond 0.3mm, the increment grows (**Figure 11**). The relationship between N_f and the increment in damage variables after the first tension suggests that, reducing the increment in damage variables after the first tension might lead to a lifespan extension of the model.

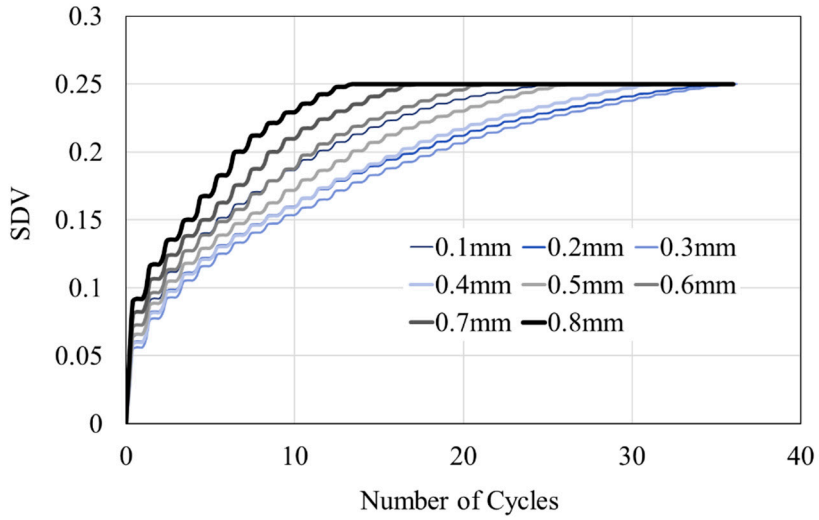

Figure 10. Variation of the damage variables of the upper right element under different resin thicknesses with increasing tension cycles.

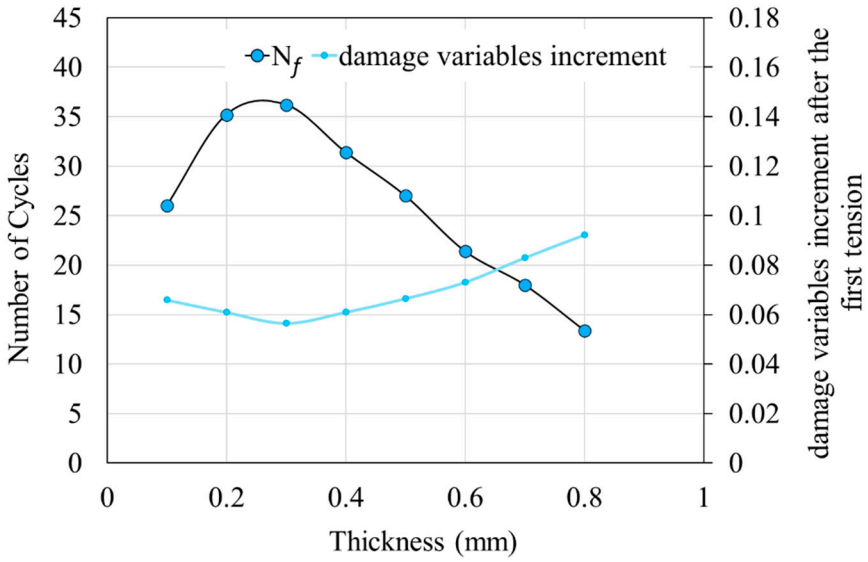

Figure 11. Relationship between the number of cycles to failure, damage variables increment after the first tension and resin thickness.

These observations suggest that when discussing the lifespan of adhesive joints, there is an optimal adhesive thickness that can maximize their durability. Yet, whether the optimal adhesive thickness of 0.3mm applies to models with different adhesive layer lengths, and what other factors might influence the ideal adhesive thickness remain subjects for further investigation.

4. Conclusions

This study discusses the stress distributions and fatigue behavior of SLS models under different adhesive layer thicknesses. The key points are summarized as follows:

(1) For the resin element under tension, the stress magnitudes consistently follow the sequence $\sigma_{22}>\sigma_{11}>\tau_{12}$. Despite the diminishing stresses across all directions with increasing tension cycles, the sequence of stress magnitudes remains unchanged.

(2) Across the adhesive interface under tension, stress peaks appear at both ends of the resin. However, as the outermost resin element fails, the nearby stress peak shift towards the center of the resin. Magnitude of these peaks is not constant but varies with increasing tensile cycles.

(3) With increasing resin thickness, N_f initially rise, then fall, peaking at 0.3mm thickness. Conversely, the increase in damage variables after the first tension shows an opposing trend.

In this study, optimal resin thickness for damage resistance appears to be around 0. 3mm. These conclusions offer valuable insights into resin-CFRP interface stress behavior and resin failure mechanisms under cyclic loading.

Acknowledgments: Parts of this study were financially supported by the JST MIRAI grant number 221036344, New Energy and Industrial Technology Development Organization (NEDO), and KAKENHI grant number 21KK0063.

References

1. A. Akhavan-Safar, F. Ramezani, F. Delzendehrooy, M.R. Ayatollahi, L.F.M. da Silva, A review on bi-adhesive joints: Benefits and challenges, Int J Adhes Adhes. 114 (2022) 103098. https://doi.org/10.1016/j.ijadhadh.2022.103098.
2. L.D.C. Ramalho, I.J. Sánchez-Arce, D.C. Gonçalves, J. Belinha, R.D.S.G. Campilho, Numerical analysis of the dynamic behaviour of adhesive joints: A review, Int J Adhes Adhes. 118 (2022) 103219. https://doi.org/10.1016/j.ijadhadh.2022.103219.
3. S. Ebnesajjad, A.H. Landrock, Adhesives Technology Handbook, Third, Elsevier Inc., Oxford, 2014. https://doi.org/10.1115/1.3225943.
4. S. Bhowmik, H.W. Bonin, V.T. Bui, R.D. Weir, Durability of adhesive bonding of titanium in radiation and aerospace environments, Int J Adhes Adhes. 26 (2006) 400–405. https://doi.org/10.1016/j.ijadhadh.2005.05.004.
5. C. V. Katsiropoulos, A.N. Chamos, K.I. Tserpes, S.G. Pantelakis, Fracture toughness and shear behavior of composite bonded joints based on a novel aerospace adhesive, Compos B Eng. 43 (2012) 240–248. https://doi.org/10.1016/j.compositesb.2011.07.010.
6. E.A.S. Marques, L.F.M. Da Silva, M. Flaviani, Testing and simulation of mixed adhesive joints for aerospace applications, Compos B Eng. 74 (2015) 123–130. https://doi.org/10.1016/j.compositesb.2015.01.005.
7. D. Quan, J.L. Urdániz, C. Rouge, A. Ivanković, The enhancement of adhesively-bonded aerospace-grade composite joints using steel fibres, Compos Struct. 198 (2018) 11–18. https://doi.org/10.1016/j.compstruct.2018.04.071.
8. J. Kupski, S. Teixeira de Freitas, Design of adhesively bonded lap joints with laminated CFRP adherends: Review, challenges and new opportunities for aerospace structures, Compos Struct. 268 (2021) 113923. https://doi.org/10.1016/j.compstruct.2021.113923.
9. S. Wang, Y. Kitamura, N. Hiraishi, S. Taira, A. Tsuge, T. Kaneko, D. Kaneko, Preparation of mussel-inspired biopolyester adhesive and comparative study of effects of meta- or para-hydroxyphenylpropionic acid segments on their properties, Polymer (Guildf). 165 (2019) 152–162. https://doi.org/10.1016/j.polymer.2019.01.012.
10. C. Xu, T. Siegmund, K. Ramani, Rate-dependent crack growth in adhesives: II. Experiments and analysis, Int J Adhes Adhes. 23 (2003) 15–22. https://doi.org/10.1016/S0143-7496(02)00063-5.
11. X.-Y. Miao, X. Chen, R. Lu, M.A. Eder, Multi-site crack initiation in local details of composite adhesive joints, Compos B Eng. 242 (2022) 110055. https://doi.org/10.1016/j.compositesb.2022.110055.

12. V. Dumont, G. Stamoulis, C. Badulescu, A. Lefèvre, D. Thévenet, Investigation of the influence of the temperature on the fracture properties of adhesive joints using the Arcan device, Eng Fract Mech. 269 (2022) 108524. https://doi.org/10.1016/j.engfracmech.2022.108524.
13. K. Ishii, M. Imanaka, H. Nakayama, H. Kodama, Fatigue failure criterion of adhesively bonded CFRP/metal joints under multiaxial stress conditions, Compos Part A Appl Sci Manuf. 29 (1998) 415–422. https://doi.org/10.1016/S1359-835X(97)00096-1.
14. K. Ishii, M. Imanaka, H. Nakayama, H. Kodama, Evaluation of the fatigue strength of adhesively bonded CFRP/metal single and single-step double-lap joints, Compos Sci Technol. 59 (1999) 1675–1683. https://doi.org/10.1016/S0266-3538(99)00028-7.
15. J.A.M. Ferreira, P.N. Reis, J.D.M. Costa, M.O.W. Richardson, Fatigue behaviour of composite adhesive lap joints, Compos Sci Technol. 62 (2002) 1373–1379. https://doi.org/10.1016/S0266-3538(02)00082-9.
16. Y. Zhang, A.P. Vassilopoulos, T. Keller, Environmental effects on fatigue behavior of adhesively-bonded pultruded structural joints, Compos Sci Technol. 69 (2009) 1022–1028. https://doi.org/10.1016/j.compscitech.2009.01.024.
17. J.H. Tang, I. Sridhar, N. Srikanth, Static and fatigue failure analysis of adhesively bonded thick composite single lap joints, Compos Sci Technol. 86 (2013) 18–25. https://doi.org/10.1016/j.compscitech.2013.06.018.
18. P.N.B. Reis, J.F.R. Monteiro, A.M. Pereira, J.A.M. Ferreira, J.D.M. Costa, Fatigue behaviour of epoxy-steel single lap joints under variable frequency, Int J Adhes Adhes. 63 (2015) 66–73. https://doi.org/10.1016/j.ijadhadh.2015.08.008.
19. B. Schneider, V.C. Beber, M. Brede, Estimation of the lifetime of bonded joints under cyclic loads at different temperatures, J Adhes. 92 (2016) 795–817. https://doi.org/10.1080/00218464.2015.1114928.
20. H. Khoramishad, A.D. Crocombe, K.B. Katnam, I.A. Ashcroft, Predicting fatigue damage in adhesively bonded joints using a cohesive zone model, Int J Fatigue. 32 (2010) 1146–1158. https://doi.org/10.1016/j.ijfatigue.2009.12.013.
21. S. Jimenez, R. Duddu, On the parametric sensitivity of cohesive zone models for high-cycle fatigue delamination of composites, Int J Solids Struct. 82 (2016) 111–124. https://doi.org/10.1016/j.ijsolstr.2015.10.015.
22. L. Ben Fekih, O. Verlinden, G. Kouroussis, Derivation of a fatigue damage law for an adhesive from in-situ bending tests, Eng Fract Mech. 245 (2021) 107587. https://doi.org/10.1016/j.engfracmech.2021.107587.
23. J. Schijve, Fatigue of structures and materials, 2009. https://doi.org/10.1007/978-1-4020-6808-9.
24. C. Basaran, S. Nie, An irreversible thermodynamics theory for damage mechanics of solids, International Journal of Damage Mechanics. 13 (2004) 205–223. https://doi.org/10.1177/1056789504041058.
25. M. Naderi, M. Amiri, M.M. Khonsari, On the thermodynamic entropy of fatigue fracture, Proceedings of the Royal Society A: Mathematical, Physical and Engineering Sciences. 466 (2010) 423–438. https://doi.org/10.1098/rspa.2009.0348.
26. M. Amiri, M.M. Khonsari, Life prediction of metals undergoing fatigue load based on temperature evolution, Materials Science and Engineering A. 527 (2010) 1555–1559. https://doi.org/10.1016/j.msea.2009.10.025.
27. G. Meneghetti, Analysis of the fatigue strength of a stainless steel based on the energy dissipation, Int J Fatigue. 29 (2007) 81–94. https://doi.org/10.1016/j.ijfatigue.2006.02.043.
28. A. Mahmoudi, M.M. Khonsari, Investigation of metal fatigue using a coupled entropy-kinetic model, Int J Fatigue. 161 (2022) 106907. https://doi.org/10.1016/j.ijfatigue.2022.106907.
29. P. Ribeiro, J. Petit, L. Gallimard, Experimental determination of entropy and exergy in low cycle fatigue, Int J Fatigue. 136 (2020) 105333. https://doi.org/10.1016/j.ijfatigue.2019.105333.
30. J. Huang, C. Li, W. Liu, Investigation of internal friction and fracture fatigue entropy of CFRP laminates with various stacking sequences subjected to fatigue loading, Thin-Walled Structures. 155 (2020) 106978. https://doi.org/10.1016/j.tws.2020.106978.
31. J. Huang, H. Yang, W. Liu, K. Zhang, A. Huang, Confidence level and reliability analysis of the fatigue life of CFRP laminates predicted based on fracture fatigue entropy, Int J Fatigue. 156 (2022) 106659. https://doi.org/10.1016/j.ijfatigue.2021.106659.
32. H.W. Lee, C. Basaran, H. Egner, A. Lipski, M. Piotrowski, S. Mroziński, N. Bin Jamal M, C. Lakshmana Rao, Modeling ultrasonic vibration fatigue with unified mechanics theory, Int J Solids Struct. 236–237 (2022). https://doi.org/10.1016/j.ijsolstr.2021.111313.
33. J. Huang, C. Li, W. Liu, Investigation of internal friction and fracture fatigue entropy of CFRP laminates with various stacking sequences subjected to fatigue loading, Thin-Walled Structures. 155 (2020) 106978. https://doi.org/10.1016/j.tws.2020.106978.
34. J. Koyanagi, A. Mochizuki, R. Higuchi, V.B.C. Tan, T.E. Tay, Finite element model for simulating entropy-based strength-degradation of carbon-fiber-reinforced plastics subjected to cyclic loadings, Int J Fatigue. 165 (2022) 107204. https://doi.org/10.1016/j.ijfatigue.2022.107204.

35. M. Sato, K. Hasegawa, J. Koyanagi, R. Higuchi, Y. Ishida, Residual strength prediction for unidirectional CFRP using a nonlinear viscoelastic constitutive equation considering entropy damage, Compos Part A Appl Sci Manuf. 141 (2021) 106178. https://doi.org/10.1016/j.compositesa.2020.106178.
36. N. Takase, J. Koyanagi, K. Mori, T. Sakai, Molecular Dynamics Simulation for Evaluating Fracture Entropy of a Polymer Material under Various Combined Stress States, Materials. 14 (2021) 1884. https://doi.org/10.3390/ma14081884.
37. T. Sakai, N. Takase, Y. Oya, J. Koyanagi, A Possibility for Quantitative Detection of Mechanically-Induced Invisible Damage by Thermal Property Measurement via Entropy Generation for a Polymer Material, Materials. 15 (2022) 737. https://doi.org/10.3390/ma15030737.
38. H. Deng, K. Toda, M. Sato, J. Koyanagi, Micro-Scale Numerical Simulation of Fatigue Failure for CFRP Subjected to Multiple-Amplitude Cyclic Loadings Based on Entropy Damage Criterion, Materials. 16 (2023) 6120. https://doi.org/10.3390/ma16186120.
39. C. Basaran, S. Nie, An irreversible thermodynamics theory for damage mechanics of solids, International Journal of Damage Mechanics. 13 (2004) 205–223. https://doi.org/10.1177/1056789504041058.
40. H. Kagawa, Y. Umezu, K. Sakaue, J. Koyanagi, Numerical simulation for the tensile failure of randomly oriented short fiber reinforced plastics based on a viscoelastic entropy damage criterion, Composites Part C: Open Access. 10 (2023) 100342. https://doi.org/10.1016/j.jcomc.2022.100342.